Chemical Engineering Journal 548 (2026) 180838

Contents lists available at ScienceDirect

Chemical Engineering Journal

journal homepage: www.elsevier.com/locate/cej

Scalable continuous-flow photocatalytic system based on a TiO_2-coated sand composite for microplastic mineralization

Carlos Company-Domenech, Alberto Blazquez-Moraleja, Francisco Bosca *, M. Luisa Marin *

Instituto de Tecnología Química (ITQ), Consejo Superior de Investigaciones Científicas-Universitat Politècnica de València, Avenida de los Naranjos, 46022 Valencia, Spain

ARTICLE INFO

Keywords:
Continuous flow-through photoreactor
Heterogeneous TiO_2 photocatalysis
Mineralization
Polyethylene terephthalate (PET) microplastics (MPs)
Silicon oxide
Sand
UVA LED

ABSTRACT

Microplastics (MPs) represent a persistent environmental threat, with polyethylene terephthalate MPs (PET) from textiles and domestic washing posing particular challenges due to their widespread use in bottles, cleaning products, and clothing fibers. While most reported photocatalysis strategies for PET degradation rely on TiO_2 suspensions, often requiring pH adjustment or chemical additives, we present here the first continuous-flow system to achieve effective mineralization of PET directly in untreated domestic washing wastewater generated without detergent addition. Accordingly, an optimized TiO_2 layer was immobilized onto commercial sand and SiO_2 microspheres, and the resulting materials were integrated to yield a structurally robust photocatalytic system (sand@TiO_2-SiO_2@TiO_2) that synergistically combines the intrinsic mechanical filtration capacity of sand with the enhanced specific surface area provided by the TiO_2-functionalized SiO_2 microspheres. This material was thoroughly characterized using FESEM, Raman, XRD, UV–Vis diffuse reflectance, and XPS. Its implementation in a lab-scale tubular photoreactor equipped with LED lamps (λ_{max} = 362 nm) demonstrated complete removal of PET microplastics from wastewater generated from domestic textile washing with tap water at a flow rate of 0.05 L h^{-1}, as confirmed by COD, TOC, gravimetry, turbidimetry, FTIR, and microscopy. Mechanistic elucidation of PET photodegradation was achieved using EPR and LC-MS. The results of this study indicate that the sand@TiO_2-SiO_2@TiO_2 photocatalyst is effective for the mineralization of microplastics in continuous-flow systems. This scalable strategy advances microplastic remediation by linking traditional laboratory-scale suspension photocatalysis research with real-world wastewater treatment applications. Moreover, this approach paves the way for the design of new advanced materials to improve microplastic removal.

1. Introduction

The widespread use of plastics in human and industrial activities has driven global production beyond 400 million tons annually, with projections to double by 2040 [1]. This surge generates significant waste, contaminating water bodies even after wastewater treatment. Estimates suggest 4.8 to 12.7 million tons of plastic are indiscriminately discarded, exacerbating environmental issues [2]. The most common plastics are polyethylene (PE), polypropylene (PP), polyamide (PA), polyethylene terephthalate (PET), polystyrene (PS), polyurethane (PU), and polyvinyl chloride (PVC), which share low degradability [3,4].

Exposure to sunlight, temperature changes, and abrasion fragments plastics (smaller than 5 mm) into secondary microplastics (MPs), while primary MPs are intentionally manufactured for cosmetics, pharmaceuticals, and personal care products [5–8]. Due to their tiny size, resilience to degradation, lax regulation, and easy dispersion, MPs persist in ecosystems in high concentrations, especially in bodies of water such as rivers, lakes, and seas [9–12]. MPs pose health risks, including intestinal damage, inflammation, metabolic disruptions, and developmental abnormalities [13–16]. Additionally, they act as vectors for pollutants like heavy metals, persistent organic pollutants, and drug-resistant bacteria, facilitating their spread and infiltration into the food chain [17–19]. In response to this issue, various strategies have been devised to mitigate microplastic pollution, employing physical, chemical, and biological treatments [20–22]. Biological approaches have resulted in microorganisms capable of breaking down the plastic surface into lower molecular weight compounds, although they require long periods of action, often as long as several months [23]. Other methods,

* Corresponding authors.
E-mail addresses: fbosca@itq.upv.es (F. Bosca), marmarin@itq.upv.es (M.L. Marin).

https://doi.org/10.1016/j.cej.2026.180838
Received 17 March 2026; Received in revised form 10 June 2026; Accepted 16 August 2026
Available online 17 August 2026
1385-8947/© 2026 The Authors. Published by Elsevier B.V. This is an open access article under the CC BY license (http://creativecommons.org/licenses/by/4.0/).

such as incineration, offer faster or more effective results but may generate more toxic by-products [24]. Further studies report changes in surface morphology, decreases in size, alteration in physicochemical properties such as surface charge or hydrophilicity, and an increase in oxygen-containing functional groups. However, these results are controversial: while increased oxygenated functional groups may enhance degradation, size reduction can exacerbate pollution by generating more problematic, smaller particles. Therefore, while all efforts to solve this global problem are valuable, these strategies have significant limitations [25].

Nevertheless, advanced oxidation processes (AOPs) have emerged as a promising alternative for treating MPs in water. These methods are effective at eliminating chemically stable and non-biodegradable pollutants [26,27]. Furthermore, AOPs can serve as a tertiary treatment in wastewater treatment plants (WWTP), helping to significantly reduce the discharge of microplastics from these facilities [28].

Currently, research is focused on validating AOPs as a reliable method for effective photodegradation of microplastics [29], particularly polyethylene terephthalate (PET). This polyester is the subject of much attention due to its widespread use in bottles, cleaning products, and clothing fibers [30,31]. Its high density and resistance to biodegradation lead to its presence in deep water, making it difficult to dispose of by conventional methods [32,33]. Moreover, PET microfibers represent a primary contaminant in wastewater from the textile industry [34], while domestic washing of clothing also contributes to microfiber release [35]. This widespread shedding of PET fibers increases their presence in both the influent and effluent of wastewater treatment plants (WWTPs) [36–40]. Various options have been explored for the photodegradation of this polymer, including photo-Fenton [38], UV-C [41], sonolysis [42], UV-H_2O_2 [40], or various photocatalysts [43–45]. Photocatalytic materials, such as TiO_2 or TiO_2-based composites, have demonstrated their promising activity for PET photodegradation [46,47]. However, they have always been performed in batch systems, and the efficiency of these methods, often based on monitoring changes in the morphology or reductions in the turbidity of the initial suspension, is limited by their low mineralization rates [48–51]. Moreover, information on kinetic degradation mechanisms and photocatalytic reactor design is insufficient [52].

Considering the above, and based on our experience in developing photocatalytic materials for the removal of organic contaminants from aqueous media [53], a new supported TiO_2-based photocatalyst was designed for continuous-flow operation, based on the hypothesis that microplastics, being organic materials with micro- and nanometric dimensions, require extended residence times on the catalyst surface to ensure effective mineralization. However, previous reports [54] within the group with unsupported SiO_2@TiO_2 microspheres showed that, despite their high specific surface area and intrinsic photocatalytic activity, their nanometric size leads to rapid excessive operational overpressure under flow-through conditions, limiting their direct applicability in packed-bed reactors. Anchoring these microspheres overcomes this limitation by combining the photocatalytic functionality of nanostructured TiO_2 with the favorable hydraulic properties of a granular support, enabling stable continuous-flow operation without excessive pressure buildup.

To this end, sand was selected as the photocatalyst support, as it is commonly employed in filtration processes for microparticles and is highly transparent within the UVA range. Accordingly, the sand was coated with an optimized titanium layer thickness (sand@TiO_2) to maximize oxidation reactions while minimizing light absorption. Moreover, to further enhance the interfacial contact area between the microplastics and the photocatalyst, silica microspheres with the optimal titanium coating thickness (SiO_2@TiO_2) [54] were chemically linked to the Ti-coated sand surface. Thereby, the resulting innovative, durable, and reusable composite material (sand@TiO_2-SiO_2@TiO_2) was assessed for the mineralization of MPs in a continuous-flow photoreactor at the laboratory scale using wastewater generated from domestic textile washing with tap water. PET degradation was monitored by the overall effluent's chemical oxygen demand (COD), TOC, gravimetry, turbidimetry, FTIR, and emission scanning electron microscopy (FESEM). Additionally, mechanistic insights into the photocatalyzed degradation of PET were obtained through EPR, fluorescence, and LC–MS studies.

2. Materials and methods

2.1. Synthesis of sand@TiO_2 photocatalysts

Using a similar protocol described in the literature to cover glass wool with titania [53], five suspensions of activated clean sand (10 g, as shown in Section 1 of the SI) in 100 mL of EtOH were sonicated for 30 min in an ultrasonic bath (FB15053, Fisherbrand) at room temperature. In parallel, solutions of 20 mL of 2-propanol with different volumes of titanium (IV) isopropoxide (10, 25, 50, 100, and 200 μL of TTIP for the synthesis of photocatalysts 1, 2, 3, 4, and 5, respectively) were sonicated for 10 min at room temperature. Next, the sand suspensions were heated to 75 °C, and the corresponding TTIP solution in 2-propanol was added dropwise. After 2 h stirring, a water-saturated airflow of 0.2 L min^{-1} was turned on, and the mixtures were allowed to react for 20 h. Finally, they were allowed to cool to room temperature, and the suspensions were filtered and washed with EtOH (3 × 50 mL). Subsequently, the obtained TiO_2 amorphous materials were calcined at 500 °C for 2 h in a muffle (More Than Heat 30–3000, Nabertherm) to obtain sand@TiO_2 photocatalysts 1, 2, 3, 4, and 5. Prior to performing any photocatalytic experiments, all freshly prepared materials were pre-irradiated in water for several hours to remove residual organic species.

2.2. Synthesis of sand@TiO_2-SiO_2@TiO_2 photocatalysts

The preparation of sand@TiO_2-SiO_2@TiO_2 photocatalysts was performed by reacting sand@TiO_2 materials 3 and 4 with SiO_2@TiO_2 microspheres.

Thereby, the first step of this synthesis was to prepare SiO_2@TiO_2 microspheres as follows: an initial synthesis of SiO_2 microspheres was carried out according to the already published Stöber method [55]. More details in Section 1 of the SI. Subsequently, these SiO_2 microspheres were employed for the synthesis of SiO_2@TiO_2 microspheres, following an already described protocol [53,54]. See details in Section 1 of the SI.

To prepare the sand@TiO_2-SiO_2@TiO_2 photocatalysts, a scaled-up protocol was used. Then, 250 g of activated clean sand (see Section 1 of the SI) was added to 1 L of EtOH at room temperature. Then, the suspension was heated to 75 °C using an antifreeze and coolant bath (Goodyear) in a rotary evaporator system operating at ambient pressure. Then, solutions of 1250 μL or 2500 μL of TTIP in 2-propanol (20 mL) were added dropwise to obtain the sand@TiO_2 amorphous materials 3 and 4, respectively, after shaking these suspensions for 2 h alone and later, for 20 h under water-saturated airflow at 0.2 L min^{-1}.

Subsequently, SiO_2@TiO_2 microspheres (750 mg) in EtOH (250 mL) were sonicated for 1 h, added to the suspensions of sand@TiO_2 amorphous material 3 and 4, and these mixtures were kept at 75 °C with a 0.2 L min^{-1} water-saturated air flow for an additional 20 h.

Finally, the suspensions were cooled to room temperature, filtered, washed with EtOH (3 × 250 mL), dried for 24 h at 100 °C, and calcined at 500 °C for 2 h (room temperature to 500 °C at 10 °C min^{-1}, More Than Heat 30–3000, Nabertherm) to obtain *ca.* 250 g of sand@TiO_2-SiO_2@-TiO_2 photocatalysts 3T and 4T. Prior to performing any photocatalytic experiments, all freshly prepared materials were pre-irradiated with LED lamps in water for several hours to remove residual organic species.

2.3. Collection and characterization of PET samples arising from domestic textile washing with tap water

Laundry wastewater samples containing microplastics (MPs) of

polyethylene terephthalate (PET) were collected from a Bosch Maxx 7 VarioPerfect washing machine. Initially, several washes of the empty drum were performed: a first wash with detergent (Dinosuper 3000 GD) at 60 °C, followed by a subsequent wash without detergent at room temperature. Then, in every washing cycle, four new mountain and trekking sweaters made of 100% recycled polyester fibers of polyethylene terephthalate (PET) (220 g/unit, half-zip Quechua Men's MH100, blue) were washed without detergent using a 63-min program at 30 °C, followed by centrifugation at 1200 rpm. Laundry wastewater was collected from the washing machine drainpipe into a 25 L tank.

A 500 mL wastewater sample was filtered through a 0.45 μm pore-size filter (TR-200140, Teknokroma), and the filtrate was analyzed by FTIR, FESEM, and proton nuclear magnetic resonance. The amount of MPs in the laundry wastewater samples was evaluated as organic material (mg O_2 L^{-1}) from chemical oxygen demand (COD) measurements (Hanna Instruments).

2.4. Photocatalytic degradation experiments

2.4.1. Studies of phenol degradation using different sand@TiO_2 and sand@TiO_2-SiO_2@TiO_2 composites

The photocatalytic activity of the different photocatalysts sand@TiO_2-SiO_2@TiO_2 and sand@TiO_2 was evaluated at room temperature by placing 5 g of every batch in glass vials containing 4 mL of an aqueous phenol solution (6.7×10^{-4} M). Each sample was irradiated with two LED lamps, $\lambda_{max} = 362$ nm, printed on circuit boards (PCBs), placed frontally at a 9 cm distance, for 20 h (see the emission spectrum of the LED lamps in Fig. S1A). The incident radiation on each vial was *ca.* 105.5 mW cm^{-2}, determined with a Gigahertz-Optik-P2110 radiometer and the corresponding detector (UV-3719-5) at 250–400 nm. Phenol photodegradation was monitored at 270 nm using a UV–Vis spectrometer (Cary 50). Dark control was performed following the same procedure. Additionally, an aqueous phenol solution was irradiated in the absence of the photocatalyst to rule out direct photolysis.

2.4.2. Studies of microplastics degradation using a photo-reactor at different flow rates

The photoreactor consisted of a tubular pyrex glass column of 2.5 cm internal diameter x 50 cm length (see its UV–Vis transmittance spectrum in Fig. S1B) packed with the sand@TiO_2-SiO_2@TiO_2 photocatalyst 3T (300 g) and four LED PCB lamps, $\lambda_{max} = 362$ nm, placed at 7 cm with an incident total light intensity of *ca.* 260.8 mW cm^{-2} (determined with a Gigahertz-Optik-P2110 radiometer and its 250–400 nm detector (UV-3719-5)). A centrifugal pump flowed 2 L of wastewater contaminated with MPs through the photoreactor at different flow rates (0.05, 0.1, and 1 L h^{-1}), and the output photoreactor water (*ca.* 1.95 L) was collected in the collection tank. Dark control was performed following the same procedure. The photodegradation of MPs was evaluated by different parameters:

- Physicochemical parameters, including pH, conductivity, and turbidity of influent and effluent samples under irradiation, were recorded at different flow rates.
- For gravimetric and morphological analysis, 0.5 L of each effluent sample was filtered through a pre-weighed 0.45 μm pore size filter (TR-200140, Teknokroma). Filters were dried and reweighed to determine the retained solid mass, and the filtered residues were subsequently analyzed by field emission scanning electron microscopy (FESEM).
- FTIR analyses were performed on the solids filtered (0.45 μm) from the influent and effluent samples (at 0.05 L h^{-1} flow rate) obtained under both irradiated and dark conditions.
- MPs mineralization was evaluated by monitoring the TOC of the different samples after passing through a 0.22 μm nylon filter. TOC measurements were performed in NPOC (Non-Purgeable Organic Carbon) mode after inorganic carbon removal, thereby minimizing potential interference from dissolved carbonate species in the hard-water matrix.
- MPs mineralization was evaluated by monitoring the COD of samples (2 mL) taken from:

1) water of the feeding tank (input water).
2) water from the photoreactor output tank at different flow rates with and without LED illumination (output water).
3) water obtained from washings of the photocatalyst placed into the photoreactor using deionized water (0.5 L × 8) and the pump in reverse mode at the flow rate of 0.05 L·h^{-1}. The photocatalyst used for these water rinsings had been initially tested in the photoreactor under dark and light conditions to treat water containing MPs.
4) water obtained from photocatalyst sonication after the washing process described above. In this case, the photocatalyst was unpacked from the photoreactor and rinsed several times using sonication for 45 min with deionized water (0.5 L × 10).

2.5. Electron paramagnetic resonance (EPR), fluorescence, and LC-MS studies to determine the MPs degradation mechanism

Different assays with sand@TiO_2-SiO_2@TiO_2 photocatalyst 3T were performed to determine the mechanisms involving the photocatalytic degradation of MPs:

- For electron paramagnetic resonance (EPR) analysis, sand@TiO_2-SiO_2@TiO_2 3T photocatalyst (32 g) was added to a vial containing a solution of DMPO (10 mM) in 10 mL of Milli-Q water. The vial was placed between two independent face-to-face LED modules (PCB), $\lambda_{max} = 362$ nm, providing an irradiance of 1350 W/m^2, and irradiated for 7 min without agitation. Dark control was maintained simultaneously under identical conditions. After, 1 mL aliquots were withdrawn and purged under a nitrogen atmosphere for 15 min at room temperature prior to measurement.
- For fluorescence detection of hydroxyl radicals using terephthalic acid (TPA), the sand@TiO_2-SiO_2@TiO_2 3T photocatalyst (32 g) was placed in 10 mL of an aqueous solution containing TPA (0.6 mM) and NaOH (2 mM). The suspension was irradiated for 7 min under the same UVA LED setup without agitation. A dark control was also prepared. After, 3 mL aliquots were collected, and fluorescence emission spectra were recorded ($\lambda_{exc} = 325$ nm).
- The water samples were collected from the photoreactor inlet and outlet under continuous light irradiation at flow rates of 1.0, 0.1, and 0.05 L h^{-1}. The samples were filtered and analyzed by LC-MS to monitor photocatalytic degradation products.

3. Results and discussion

3.1. Identification of the most efficient sand@TiO_2-SiO_2@TiO_2 photocatalysts

In this study, new photocatalysts (sand@TiO_2-SiO_2@TiO_2) based on a TiO_2 shell supported on sand and SiO_2 microspheres were synthesized to remove microplastics from wastewater. In this context, sand was selected as the primary support for the sand@TiO_2-SiO_2@TiO_2 photocatalysts due to its intrinsic mechanical filtration capacity, negligible UV-A absorption, mechanical robustness, chemical stability, ease of recovery, and compatibility with packed-bed reactor configurations, making it well-suited for continuous-flow photocatalytic applications [56,57]. SiO_2 microspheres were used as a secondary support incorporated into the sand to enhance the density of TiO_2 active sites in the photocatalysts, as they have a much higher specific surface area than sand. In addition, optimizing the TiO_2 shell thickness on supports was needed to improve the photocatalyst's degradation efficiency [53,54]. In fact, previous studies have evidenced that TiO_2 thicknesses in the 20–40 nm range provided the best photo-reactivity of SiO_2@TiO_2 composites

[53,54]. Thus, our objective was to obtain a photocatalyst of sand@-TiO_2-SiO_2@TiO_2 with a TiO_2 shell thickness within this range. Hence, for the preparation of sand@TiO_2-SiO_2@TiO_2 photocatalysts, sand@-TiO_2 materials were reacted with SiO_2@TiO_2 microspheres in a developed multistep process, as illustrated in Scheme 1.

To prepare SiO_2@TiO_2 microspheres, the first step was to synthesize SiO_2 microspheres by a Stöber-type procedure [55], yielding monodisperse particles with an average diameter of 508 ± 23 nm (Fig. S2A) that provided a uniform, well-defined platform for subsequent TiO_2 shell coating. Hence, the amount of TTIP required for the coating process was estimated based on their average diameter, following the methodology outlined in a previous study [53]. This calculation was designed to produce SiO_2@TiO_2 spheres with a complete TiO_2 shell approximately 20 nm thick. After the synthesis and subsequent calcination of SiO_2@-TiO_2 microspheres, TEM images confirmed the formation of a uniform TiO_2 shell of *ca.* 18 nm (Fig. S2). The synthetic process preserved the original spherical morphology of SiO_2 microspheres, which now exhibited an increased average diameter of 544 ± 24 nm. Furthermore, other measurements, including Raman spectroscopy, X-ray diffraction, or X-ray Photoelectron Spectroscopy (XPS), confirmed the presence of TiO_2 on the microspheres (Fig. S3).

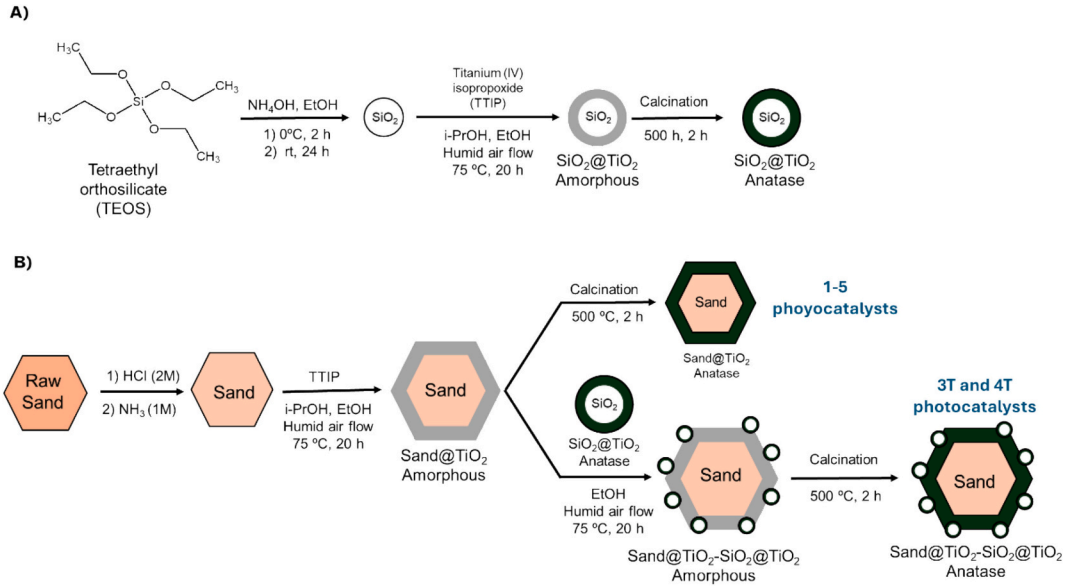
To obtain sand@TiO_2, sand was initially treated with acid (2 M HCl), followed by base, to enhance its nucleophilicity for the subsequent reaction with titanium (IV) isopropoxide (TTIP). However, the irregular grain geometry of sand prevented a reliable theoretical prediction of the TiO_2 thickness from the precursor amount, necessitating experimental optimization. Hence, a series of sand@TiO_2 photocatalysts (1–5) was prepared by reacting 10 g of activated sand with increasing volumes of TTIP (10, 25, 50, 100, and 200 μL, respectively) under identical experimental conditions, resulting in progressively thicker coatings on the activated sand. The coating strategy, which ensured intimate contact between TTIP and the activated sand surface before hydrolysis, enhanced TiO_2 coating and avoided the multiple coating cycles often required in alternative approaches, which are typically more time- and energy-consuming [56,57]. Morphological analysis by FESEM showed that this procedure yielded continuous TiO_2 layers on sand without visible cracking for all members of the sand@TiO_2 series (Fig. S4), demonstrating the mild and reproducible nature of the coating process.

The impact of TiO_2 coating thickness on photocatalytic performance was subsequently evaluated using phenol as a model pollutant [58] (6.7×10^{-4} M) under UVA irradiation at 362 nm in aerated aqueous conditions. Phenol degradation was monitored by UV–Vis spectroscopy at 270 nm (Fig. S5A shows the phenol absorption spectrum), and negligible phenol adsorption was detected under dark conditions for all materials (see more details in Fig. S5B), confirming that the concentration decrease under irradiation arises from photocatalytic degradation rather than adsorption. Hence, phenol removal increased with TiO_2 loading up to sand@TiO_2 3 and decreased for higher precursor amounts, revealing an optimal coating thickness within the series (Fig. 1A.). A focused ion beam analysis of the representative sand@TiO_2 3 sample confirmed complete coverage of the sand grains, albeit with a non-uniform TiO_2 thickness ranging from *ca.* 10 to 70 nm. Fig. 1C. shows a representative electron microscopy image of the sand@TiO_2 photocatalyst 3, along with cross-sectional views obtained after focused ion beam (FIB) preparation. Since TiO_2 thickness is the only parameter that varies among these materials, this trend is attributed to the balance between light absorption and charge carrier generation *versus* recombination, in agreement with previous studies on supported TiO_2 materials [54]. These observations highlight the intrinsic differences between regular spherical supports and irregular granular substrates and emphasize the need to experimentally optimize TiO_2 thickness when designing sand-based photocatalysts.

On the basis of the phenol degradation results, sand@TiO_2 photocatalysts 3 and 4 were selected as the most promising candidates to further increase the active surface area by decorating them with SiO_2@TiO_2 microspheres. Thus, by applying the second synthetic procedure described in Scheme 1B., sand@TiO_2 3 and 4 were transformed into the corresponding sand@TiO_2-SiO_2@TiO_2 photocatalysts 3T and 4T, respectively. Both materials were first evaluated in the photocatalytic degradation of phenol under UVA irradiation at 362 nm, under the same conditions used for the sand@TiO_2 series (Fig. 1B.). As anticipated, both 3T and 4T showed significantly higher activities than their sand@TiO_2 precursors, and 3T was identified as the most efficient heterogeneous photocatalyst in this series. Consequently, sand@TiO_2-SiO_2@TiO_2 3T was selected for detailed characterization and for subsequent microplastic mineralization studies in continuous flow.

3.2. *Characterization of sand@TiO_2-SiO_2@TiO_2 photocatalyst 3T*

The presence of TiO_2 in sand@TiO_2-SiO_2@TiO_2 3T and in its precursor sand@TiO_2 3 was first assessed by UV–Vis diffuse reflectance spectroscopy (Fig. 2A.). Both materials exhibited increased absorption in the 250–370 nm region compared to clean sand, consistent with the presence of TiO_2. When comparing sand@TiO_2-SiO_2@TiO_2 3T with



Scheme 1. Synthesis of (A) SiO_2@TiO_2 microspheres and (B) sand@TiO_2 photocatalysts (1–5) and sand@TiO_2-SiO_2@TiO_2 photocatalysts (3T and 4T).

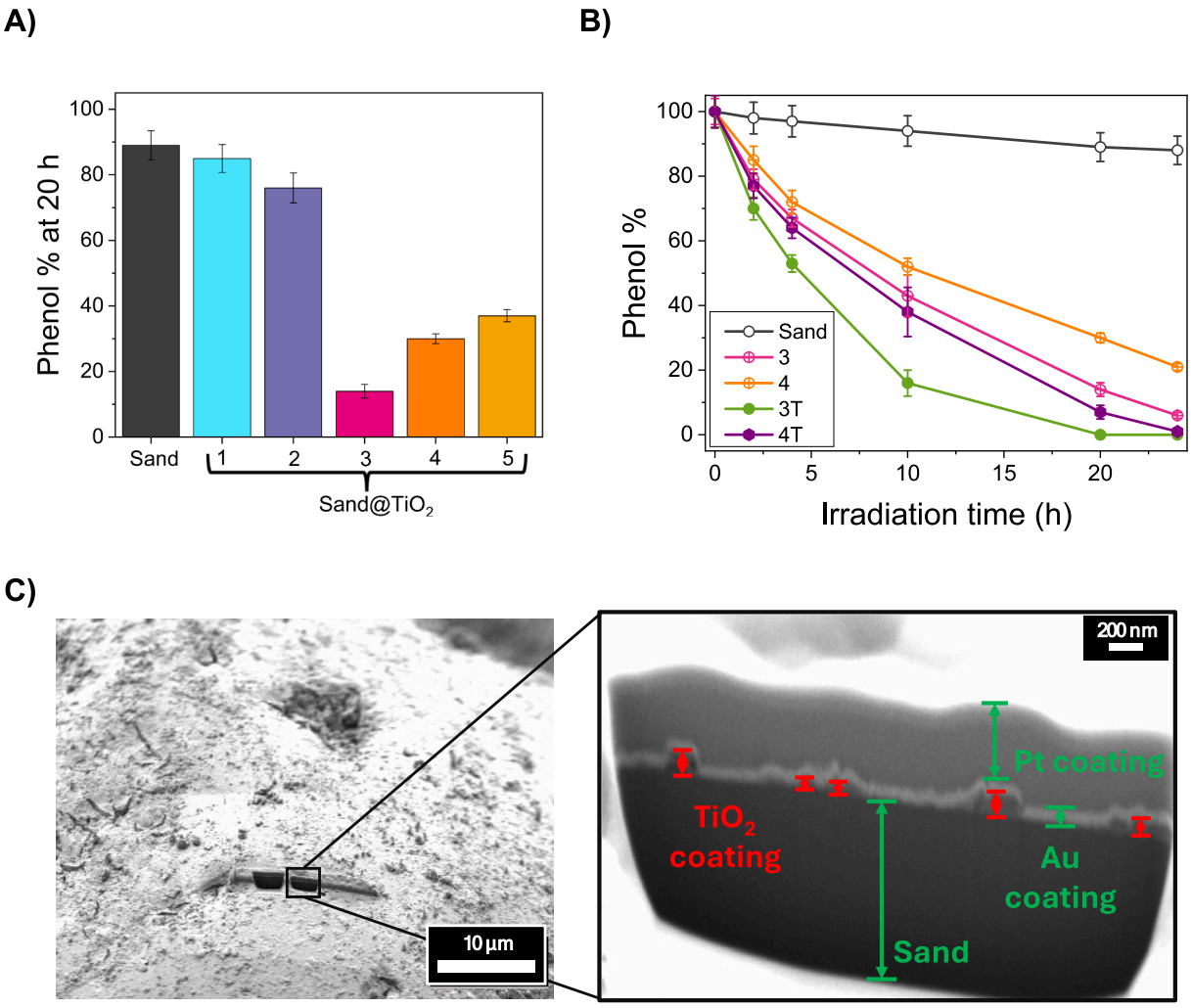


Fig. 1. (A) Phenol (6.7×10^{-4} M, 4 mL) remaining (%) after 20 h irradiation with two PCB LED lamps (λ_{max} = 362 nm) for 5 g of bare sand and the sand@TiO_2 photocatalysts 1–5. (B) Phenol (6.7×10^{-4} M, 4 mL) remaining (%) during irradiation time with two PCB LED lamps (362 nm) for 5 g of bare sand and the sand@TiO_2 photocatalysts 3, 4 and sand@TiO_2-SiO_2@TiO_2 photocatalyst 3T and 4T. (C) Representative electron microscopy images of the sand@TiO_2 photocatalyst 3. Left: Low magnification image showing the selected sand grain. Right: Cross-sectional view obtained after preparation with focused ion beam (FIB).

sand@TiO_2 3, a pronounced additional absorption in this UV region was observed, attributed to the extra TiO_2 introduced *via* the SiO_2@TiO_2 microspheres, although this technique is not quantitative. Kubelka-Munk transformed spectra for sand@TiO_2 3 and 3T (Fig. 2B.) showed nearly identical apparent band gaps, which is consistent with the similar nature of the titania coating the silica supports and the comparable size of TiO_2 nanocrystals in SiO_2@TiO_2, sand@TiO_2, and sand@TiO_2-SiO_2@TiO_2.

X-ray photoelectron spectroscopy confirmed the presence of titanium on the surface of sand@TiO_2-SiO_2@TiO_2 3T (Fig. 2C.). The Ti 2p spectrum displayed two main peaks at 458.5 eV (Ti $2p_{3/2}$) and 464.2 eV (Ti $2p_{1/2}$), referenced to C 1s at 284.5 eV, with a spin-orbit splitting of 5.7 eV and an area ratio of approximately 2:1, in agreement with Ti(IV) in anatase TiO_2 [59]. FESEM images of sand@TiO_2-SiO_2@TiO_2 3T after calcination revealed a dense distribution of microspheres adhered over the entire sand surface (Fig. 2D.), and EDS elemental mapping of O, Si, and Ti showed a homogeneous Ti signal on the composite, corroborating the spectroscopic evidence for uniform TiO_2 coverage (Fig. 2E.). The wt % of TiO_2 determined by ICP-OES revealed a very low value of 0.089 ± 0.001%.

To further investigate the crystalline phase of TiO_2, Raman spectroscopy and X-ray diffraction were performed on sand@TiO_2-SiO_2@TiO_2 3T (Fig. S6). In this case, the typical anatase bands and reflections were not discernible, and the spectra closely resembled those of quartz-rich sand [60,61], which can be ascribed to the very low titania-to-sand ratio in the composite. In contrast, Raman and XRD analyses of SiO_2@TiO_2 microspheres prior to their immobilization onto sand clearly evidenced anatase TiO_2, and the crystallite size was estimated to be *ca.* 12 nm from the diffraction peak at 25° using the Scherrer equation [62] (Fig. S3). N_2 adsorption-desorption measurements on sand@TiO_2-SiO_2@TiO_2 3T were inconclusive due to the extremely low total surface area (<0.1 m^2 g^{-1}), falling below the sensitivity of the equipment; similarly, photocurrent measurements did not yield measurable signals for the same reason.

Photoluminescence (PL) spectroscopy was employed to probe the photophysical behavior of TiO_2 in sand@TiO_2 3 and sand@TiO_2-SiO_2@TiO_2 3T (Fig. S7). However, clean sand exhibited a strong emission band centered at *ca.* 430 nm, very close to the typical emission of TiO_2 nanocrystals (around 450 nm), and with an intensity higher than that of the TiO_2-containing composites. As a result, the overall PL response was dominated by the sand contribution, and the observed decrease in emission intensity upon increasing TiO_2 coverage reflects a reduced relative contribution of the sand signal rather than a genuine decrease in charge carrier recombination within TiO_2. Consequently, PL was not considered suitable for quantifying recombination in these low-loaded materials.

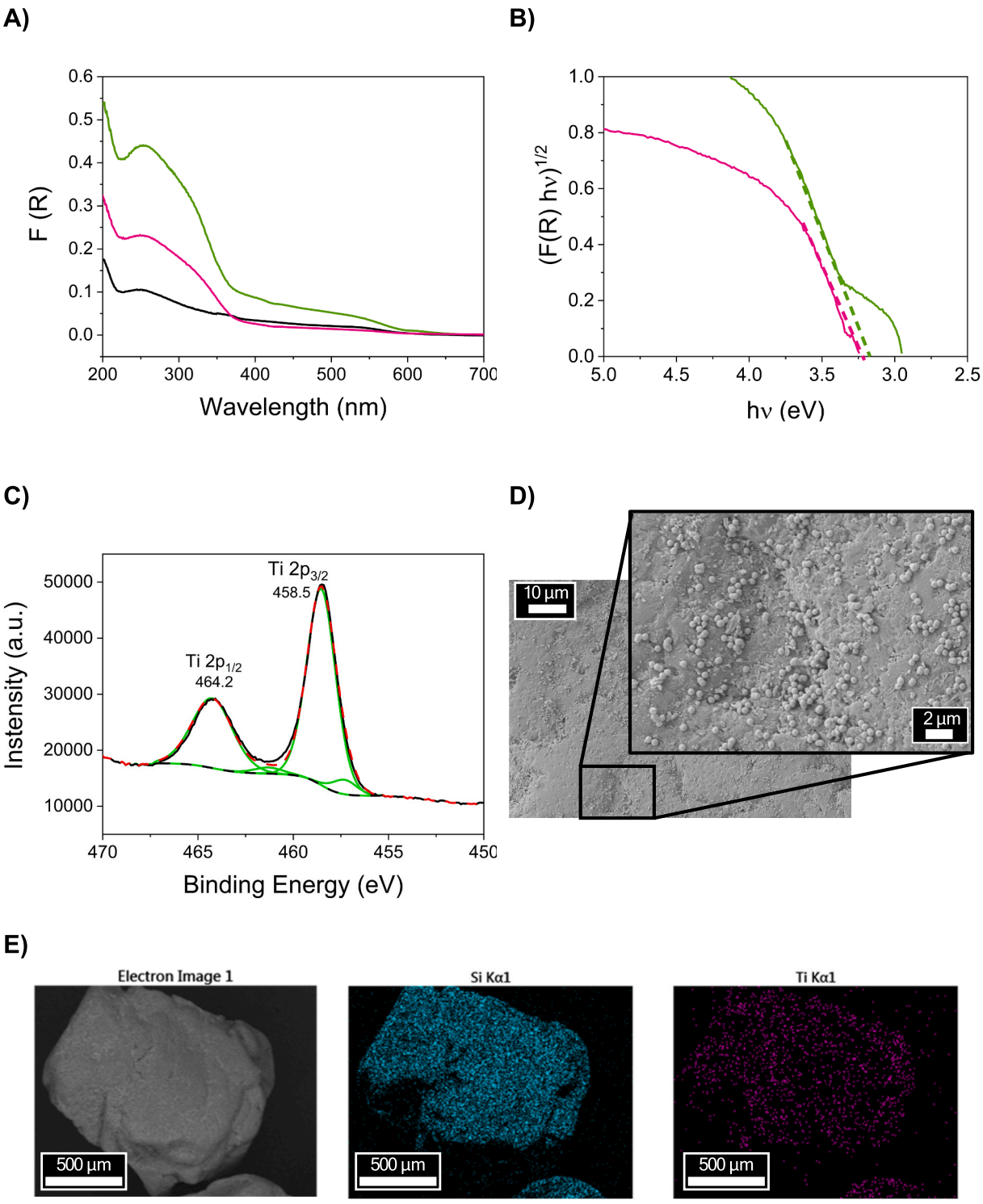


Fig. 2. (A) Diffuse UV reflectance spectra of clean sand (black), sand@TiO_2 3 (pink), and photocatalyst sand@TiO_2-SiO_2@TiO_2 3T (green). (B) Kubelka-Munk transformed diffuse reflectance spectra for sand@TiO_2 3 (pink) and photocatalyst sand@TiO_2-SiO_2@TiO_2 3T (green) after using the diffuse UV reflectance of clean sand as a baseline for both photocatalysts; dashed lines indicate the linear fits used for the band gap determination. (C) X-ray photoelectron spectroscopy (XPS) spectrum of Ti 2p from the photocatalyst sand@TiO_2-SiO_2@TiO_2 3T, showing the Ti $2p_{3/2}$ and Ti $2p_{1/2}$ components. (D) FESEM images of the surface of photocatalyst sand@TiO_2-SiO_2@TiO_2 3T at different magnifications. (E) FESEM-EDS analysis of the photocatalyst sand@TiO_2-SiO_2@TiO_2 3T, including electron imaging and elemental mapping of the Si and Ti elements.

3.3. Collection and characterization of MPs

One of the main challenges in microplastics research is their limited commercial availability, which has led many studies to rely on artificially generated particles or model polymer powders rather than realistic waste streams [45,50,63–68]. In this work, real microplastic samples were deliberately used to better reproduce the conditions encountered in wastewater treatment plants. Recycled polyester garments (100% PET) were washed with tap water without detergent, and the resulting laundry wastewater was collected as described in Section

2.3. The absence of detergent allowed the specific evaluation of PET microplastic degradation under high-ionic-strength conditions while minimizing competitive ROS scavenging and photocatalyst fouling effects associated with surfactants. The PET microfiber concentration in wastewater was determined gravimetrically after filtration, washing with Milli-Q water, and drying, yielding an average of ~31 mg L^{-1}, underscoring domestic laundry as a significant source of MPs release into wastewater systems. This realistic composition of ~31 mg L^{-1} microplastics in a highly mineralized hard-water matrix typical of domestic wastewater contrasts sharply with most photocatalytic studies reported in the literature (Table 2), which employ artificially prepared suspensions of MPs in deionized water and often in alkaline media or in the presence of additives.

Morphological characterization of the collected microplastics by FESEM showed that the samples consist predominantly of elongated PET microfibers with irregular surfaces and variable lengths (Fig. S8). However, tap water in Valencia (Spain) is known for its high concentration of calcium, sodium, and magnesium salts (see Table S1), which tend to accumulate on the fiber surface and partially mask the polymer morphology. To accurately observe the microfiber morphology by FESEM, the filters were therefore washed with Milli-Q water (4 × 100 mL) and re-filtered, which removed most inorganic deposits and revealed clean PET fibers with well-defined contours (Fig. S8B).

Chemical analysis of the recovered microplastics corroborated their chemical composition. IR spectroscopy (Fig. S9A) identified PET chemical bonds, with key absorption bands at 1721 cm^{-1} (C=O), 1245 cm^{-1} and 1100 cm^{-1} (C—O), and 2863 cm^{-1} (C—H) [45]. Proton NMR (^{1}H NMR) further confirmed the PET structure, showing characteristic aromatic (8.08 ppm) and alkyl proton signals (4.67 ppm) (Fig. S9B).

3.4. MPs degradation in a continuous flow photoreactor

At this point, degradation of domestic laundry wastewater containing PET microfibers was evaluated under continuous-flow conditions using a laboratory-scale packed-bed photoreactor using the most efficient sand@TiO_2-SiO_2@TiO_2 photocatalyst 3T. The reactor designed for this aim is shown in Fig. 3. It consisted of a tubular borosilicate glass column (total volume 245 cm^3, internal diameter 2.5 cm, length 50 cm) packed with 300 g of photocatalyst, corresponding to an effective hydraulic volume (V) of *ca.* 133 cm^3, surrounded by four LED PCB modules (L1-L4, λ_{max} = 362 nm) [53] and connected to a centrifugal pump and two tanks serving as feed and collection vessels. In this configuration, the sand@TiO_2-SiO_2@TiO_2 photocatalyst 3T acts, due to its sand component, as a robust, highly water-permeable support that, through its intrinsic mechanical filtration capacity, traps microplastic fibers within the packed bed while the TiO_2 coating on the sand and SiO_2@-TiO_2 microspheres constitutes the photocatalytically active phase responsible for the oxidation of microplastics under UVA irradiation. Pressure-drop measurements across the packed bed remained low within the investigated flow-rate range, with values of 0.13 bar at 1.0 L h^{-1} and 0.10 bar at lower flow rates (0.1 and 0.05 L h^{-1}).

To further ensure homogeneous irradiation of sand@TiO_2-SiO_2@-TiO_2 photocatalyst 3T, the number and arrangement of the LED modules were optimized using an aqueous rhodamine B solution (1.25×10^{-5} M) as a fluorescent probe, revealing that light from a single module penetrated only about half of the column diameter (Fig. S10), so four modules were finally placed symmetrically, with two modules facing the other two, to achieve full radial irradiation along the entire reactor length and maximize photocatalytic utilization of the packed bed (Fig. 3).

It is worth noting that the domestic laundry wastewater used in this study originates from a region characterized by very hard tap water, representative of a chemically complex, highly ionic matrix. As shown by the water quality analysis of the local supplier (Table S1) [69], the feed water exhibits an electrical conductivity of approximately 850–860 μS cm^{-1} and contains high concentrations of divalent cations and accompanying anions, corresponding to a total hardness in the range of 300–450 mg L^{-1} as $CaCO_3$. Consequently, the photocatalytic experiments were conducted under realistic conditions, in which PET microfibers coexist with elevated levels of inorganic ions, thereby allowing the

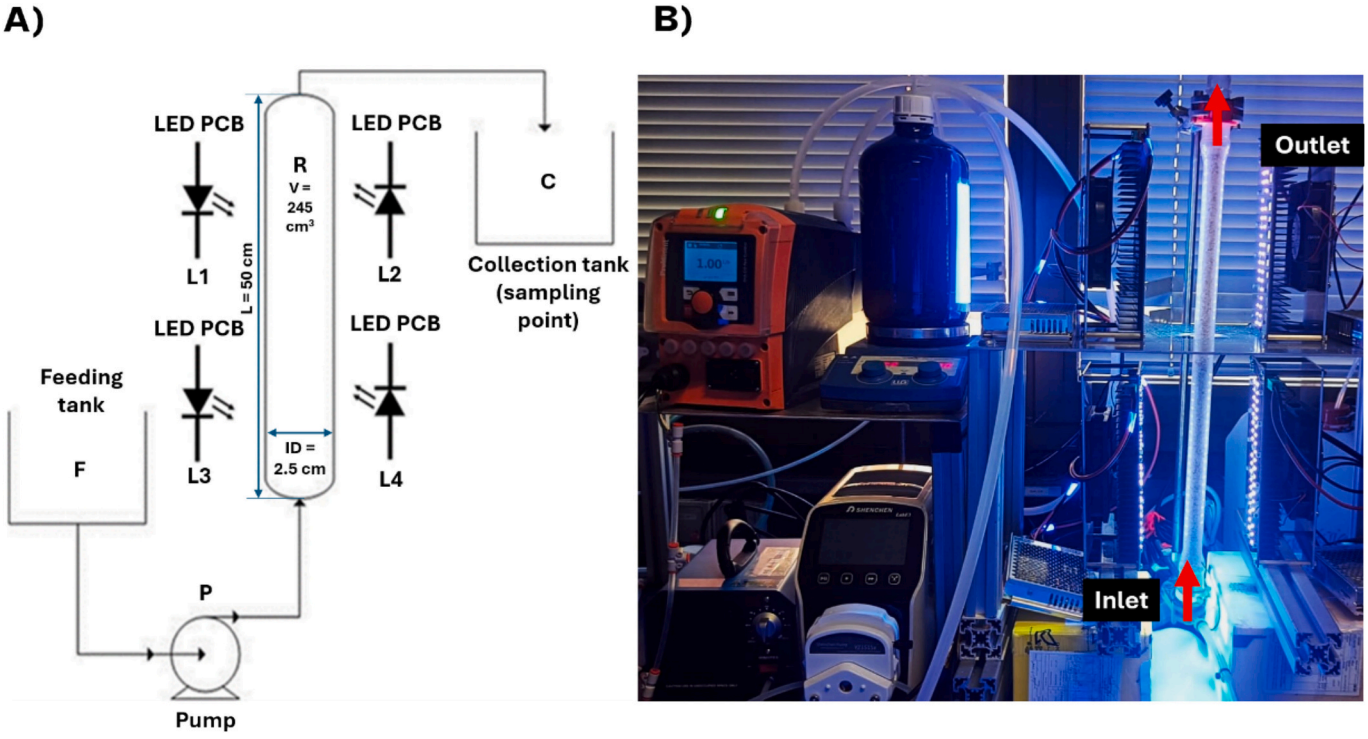


Fig. 3. A) Schematic of the lab-scale continuous-flow photoreactor. Reactor (R), LED PCB lamps (L), pump (P), feeding tank (F), and collection tank (C). B) Photograph of the assembled continuous flow photoreactor packed with the photocatalyst sand@TiO_2-SiO_2@TiO_2 3T.

system's performance to be assessed in a representative real-wastewater matrix.

The continuous-flow experiments were designed to identify operating conditions that ensure the removal of PET microplastics from the output water through a combination of filtration and photodegradation. For each experiment, 2 L of real laundry wastewater (initial COD *ca.* 133 mg O_2 L^{-1}) was circulated through the packed bed at three different flow rates (1.0, 0.1, and 0.05 L h^{-1}), corresponding to progressively increasing residence times, while maintaining identical irradiation conditions. The output water was comprehensively characterized by COD, TOC, gravimetry, and turbidity, along with basic water quality indicators (pH and conductivity), providing a detailed assessment of microplastic removal and organic matter mineralization (see Table 1). In particular, the combined use of COD and TOC analyses allows a more reliable assessment of photocatalytic mineralization than does a single analytical parameter alone. COD measurements exhibit high sensitivity to residual oxidizable organic species across a broad concentration range, including dissolved intermediates and small suspended particles, whereas TOC analysis directly evaluates residual organic carbon after filtration. Thus, the combination of these complementary methodologies, together with gravimetric and microscopic analyses, is particularly relevant to distinguish true mineralization from the mere formation of smaller microplastic or nanoplastic fragments during photocatalytic treatment. For this study, a control experiment using light and sand without the photocatalyst was not considered necessary, as only a very small fraction of the PET microplastic surface would have undergone partial oxidation, since PET exhibits negligible light absorption above 350 nm. Therefore, direct photolysis would not be expected to result in any measurable PET mineralization. Furthermore, differences in the surface properties of the sand with and without the titanium dioxide coating would also affect the adsorption of the microplastics and, consequently, the COD values measured at the reactor outlet.

Experiments in darkness were systematically conducted at all three flow rates (1.0, 0.1, and 0.05 L h^{-1}) to determine the purely physical retention (Fig. 4A., dark blue bars). As expected, the extent of microplastic retention increased with decreasing flow rate, reflecting the longer residence time within the packed bed. At the lowest flow rate (0.05 L h^{-1}), which represents our upper limit of physical retention, the COD of the output water remained around 40 mg O_2 L^{-1}, which is significantly higher than the tap water value. This indicates that a large fraction of PET microfibers was physically trapped within the packed bed under dark conditions. The difference between the COD of the water input (*ca.* 133 mg O_2 L^{-1}) and that of the dark water output at 0.05 L h^{-1} corresponds to a COD equivalent of *ca.* 93 mg O_2 L^{-1}, meaning that about 70% of the initial microplastic load is intercepted by the sand-based filter in the absence of light, in good agreement with the retention efficiencies typically reported for sand filters in wastewater treatment plants [70,71].

Under UVA irradiation, the behavior of the system becomes strongly dependent on the flow rate, which determines the effective residence time of microplastics in contact with the photocatalyst surface (Fig. 4A.). Considering the effective hydraulic volume (V) of the packed bed (133 cm^3) and the tested flow rates (Q) of 1.0, 0.1, and 0.05 L h^{-1}, the corresponding hydraulic residence times ($\tau = V/Q$) are *ca.* 8 min, 80 min, and 160 min, respectively. These results indicate that sufficient contact time between the retained MPs and the irradiated photocatalytic surface is critical for achieving extensive mineralization under continuous-flow conditions. At flow rates of 1.0 and 0.1 L h^{-1}, COD values measured at the reactor outlet remain in the same order of magnitude, and TOC data indicate only partial mineralization. This behavior is consistent with a scenario in which larger microplastic fragments are efficiently retained within the packed bed, whereas smaller particles (*i.e.*, nanoplastics) and dissolved organic intermediates are only partly degraded and can exit the reactor (Table 1). In contrast, at the lowest flow rate of 0.05 L h^{-1}, the COD of the output water drops below the analytical method's detection limit ($\leq$ 5 mg O_2 L^{-1}). In this context, the TOC value obtained also supports the MPs mineralization within analytical uncertainty. Moreover, turbidity and filtered mass also decrease to negligible levels, demonstrating effective removal of both particulate and dissolved organic carbon under these optimal conditions (Table 1 and Fig. S11). Solid-phase analyses further corroborate these trends. Thus, FESEM images of filters corresponding to the water input show abundant PET microfibers, whereas under irradiation with LED lamps, only sparse residual fragments are observed at 1.0 and 0.1 L h^{-1}, while no fibers are detected in the effluent at 0.05 L h^{-1} (Fig. 5 A-D.). In the FTIR analysis, the spectra of the solids recovered from the input water and from output water under dark conditions display the characteristic PET bands, while these fingerprints disappear when the LED light at the flow rate of 0.05 L h^{-1} is applied, indicating effective polymer degradation (see Fig. 5E.). Importantly, pH and conductivity remain essentially unchanged upon treatment, indicating that the photocatalytic process does not significantly alter the ionic composition of the water (Table 1).

To rationalize this flow-rate-dependent behavior in physically meaningful terms, COD values of the output water were subsequently replotted as a function of the hydraulic residence time (τ) (Fig. S12). This representation shows that increasing τ results in progressively lower COD values under LED irradiation, whereas the dark experiments define the upper limit for purely physical retention. These results indicate that the performance of the packed-bed photoreactor is primarily governed by residence-time and contact-time limitations rather than by flow rate *per se*, highlighting the critical role of sufficient hydraulic residence time for effective photocatalytic oxidation under continuous-flow conditions. Under optimal operating conditions (0.05 L h^{-1}, τ = 160 min), the estimated energy consumption, including both LED irradiation and pumping, was *ca.* 5767 kWh m^{-3} of mineralized wastewater.

The absence of detectable PET in the irradiated effluent demonstrates that a flow rate of 0.05 L h^{-1} is required to prevent the release of microplastic fragments from the photoreactor. However, this observation alone does not guarantee complete photodegradation of the MPs physically retained within the packed bed. To quantify the fate of these trapped particles, a dedicated recovery protocol was implemented after each run, consisting of sequential photocatalyst washing with deionized water followed by its unpacking and water sonication to dislodge strongly retained material (Fig. 4B. and Fig. S13). The combined water fractions were analyzed by COD, allowing the amount of non-mineralized organic carbon remaining inside the reactor to be

Table 1
Water quality parameters (pH, conductivity, turbidity, filtered mass, TOC, and COD) in water samples containing MPs before (input water) and after (output water) photocatalytic treatment with LED light at different flow rates. The photoreactor contained photocatalyst sand@TiO_2-SiO_2@TiO_2 3T. The values for tap water have been included for comparison.

			Output water treated with LED light at different flow rates		
	Tap water	Input water	1 L h^{-1}	0.1 L h^{-1}	0.05 L h^{-1}
pH	7.73	8.18	8.36	8.28	8.35
Conductivity (μS cm^{-1})	853.7 ± 2.1	837.7 ± 1.5	842.1 ± 2.1	839.7 ± 2.1	836.1 ± 1.1
Turbidity (FNU)	2.29 ± 0.33	11.97 ± 0.36	1.96 ± 0.71	1.46 ± 0.25	0.99 ± 0.07
Filtered mass (mg)[a]	<0.1[b]	15.3	0.5	0.1	<0.1[b]
TOC (ppm)	1.99 ± 0.04	77.16 ± 1.57	38.87 ± 0.91	27.21 ± 0.88	3.07 ± 0.01
COD (mg O_2 L^{-1})	<5[c]	133.25 ± 16.03	33.1 ± 1.4	16.5 ± 0.7	<5[c]

[a] From 500 mL samples.
[b] Detection limit of the analytical balance used for gravimetric measurements (Mettler Toledo XS204): 0.1 mg.
[c] Detection limit of the Hanna Instruments low range rapid tests used for COD determination: 5 mg O_2 L^{-1}.

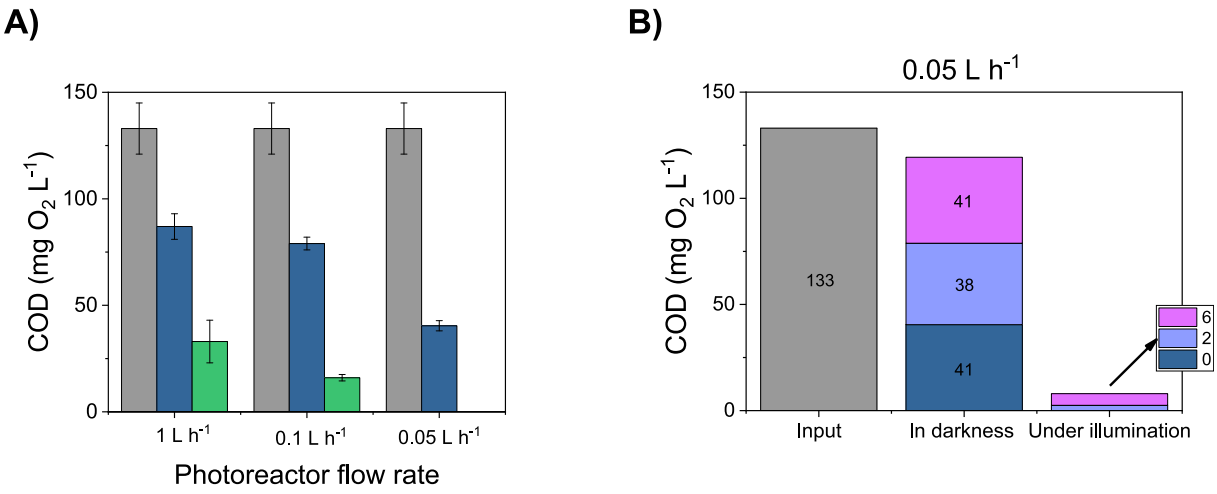


Fig. 4. (A) COD values of the input water (grey) and the photoreactor output water at different flow rates (1 L h^{-1}, 0.1 L h^{-1}, and 0.05 L h^{-1}) using photocatalyst sand@TiO_2-SiO_2@TiO_2 3T in darkness (dark blue) and under illumination with LED light centered at 362 nm (green). (B) COD value of the input water (grey) and cumulative COD values resulting from the different fractions: (i) the output water of the photoreactor packed with the sand@TiO_2-SiO_2@TiO_2 3T photocatalyst (blue), (ii) water from the photocatalyst cumulative washing steps (light blue), and (iii) water from the cumulative photocatalyst sonication treatments (pink). The results come from experiments conducted at the optimal flow rate of 0.05 L h^{-1} under dark conditions or using LED lamps.

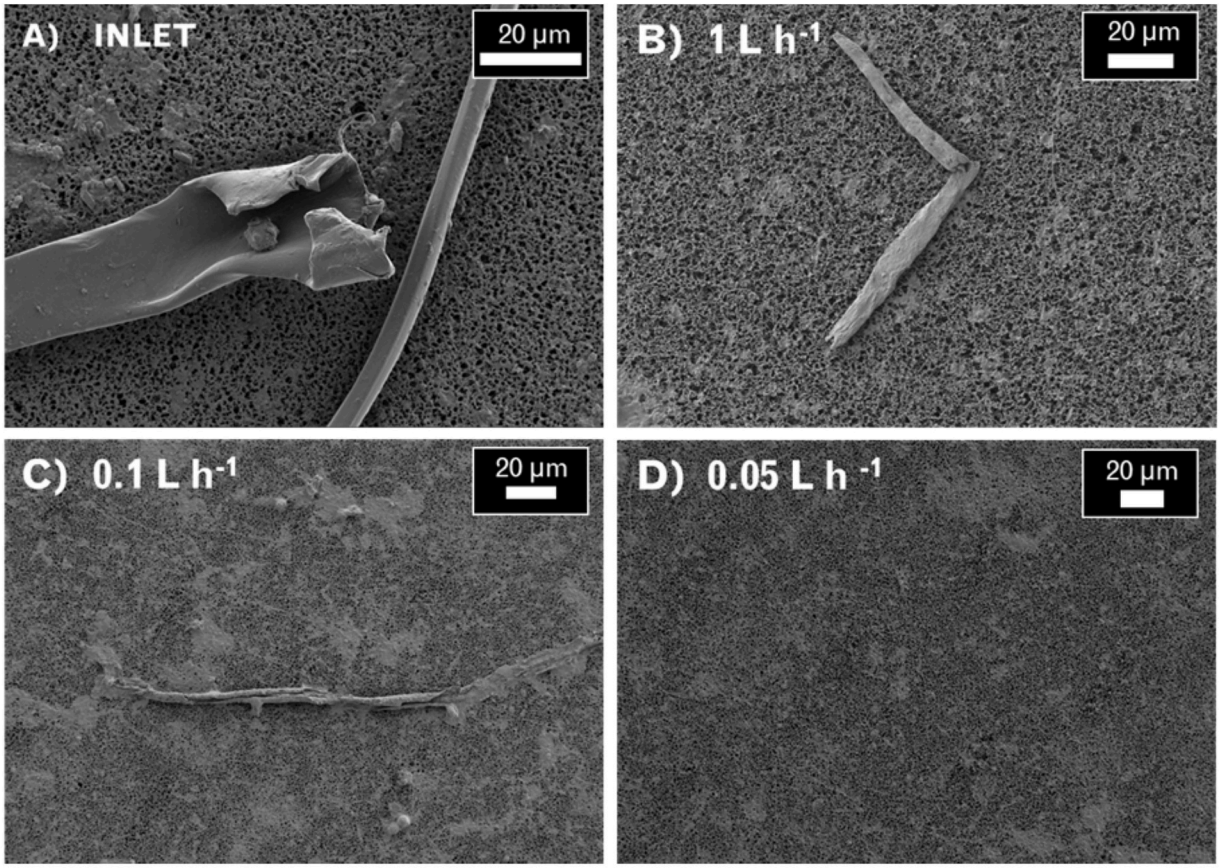
quantified. Thus, when applied to a dark experiment at 0.05 L h^{-1}, the recovery protocol (see Section 2.4) yielded a COD corresponding to *ca.* 85% of the MPs retained in the packed bed, confirming the efficiency of the recovery procedure (Fig. S13). In sharp contrast, after UVA irradiation at the same flow rate, the COD associated with the recovered fractions decreased dramatically to *ca.* 8 mg O_2 L^{-1}, indicating that only a small residual amount of MPs or microplastic-derived intermediates remained within the reactor (see light blue and pink bars in the corresponding darkness and illumination columns in Fig. 4B. and Fig. S13). The residual amount recovered from the column after irradiation at a flow rate of 0.05 L h^{-1} could be primarily attributed to the existence of a partially illuminated region along the 50 cm packed bed. As the axial photon flux distribution was not fully optimized for continuous-flow operation, a slightly lower irradiance is expected in the central section of the column due to the separation between the two vertical lamps (see Fig. 3). By combining the COD of the input water, the output water, and the water fractions of the recovered MPs after photocatalytic treatment, the overall mineralization efficiency at 0.05 L h^{-1} is estimated at approximately 95%, demonstrating that the sand@TiO_2-SiO_2@TiO_2 photocatalyst 3T retains PET microplastics but under illumination at the flow rate of 0.05 L h^{-1} produces the extensive oxidation and mineralization of them.

Overall, these results highlight the dual role of the sand-based composite as both an efficient physical filter and an active photocatalyst, preventing the release of smaller, potentially more hazardous nanoplastic fragments while converting most of the microplastic-derived organic carbon into inorganic species. Multiple continuous-flow experiments were performed using successive 2 L wastewater feeds under different operating conditions, processing more than 50 L of MPs-contaminated water with the same 300 g batch of sand@TiO_2-SiO_2@TiO_2 photocatalyst 3T. After each treatment cycle, the packed bed was regenerated by calcination prior to reuse. COD removal efficiencies before and after regeneration remained within experimental deviation, indicating stable photocatalytic performance during prolonged operation. FESEM imaging and EDS elemental mapping confirmed the preservation of the composite structure and the absence of detectable detachment of SiO_2@TiO_2 microspheres after repeated use (Fig. S14). ICP-OES analysis of the recovered photocatalyst after 50 L of mineralized wastewater indicated a value of 0.094 ± 0.004% wt TiO_2. Although this value is slightly higher than that recorded for the as-made photocatalyst, the difference is within the error. Additionally, ICP-OES analyses of the treated effluents showed Ti concentrations below the instrumental detection limit (LOD = 2 μg L^{-1}), supporting negligible Ti leaching during operation. These results indicate that the relatively high photocatalyst mass employed in the packed-bed configuration contributes not only to efficient MPs retention and homogeneous irradiation throughout the reactor, but also to the mechanical robustness and straightforward recovery/reuse of the immobilized photocatalytic phase under continuous-flow operation.

3.5. *Proposed mechanism for MPs degradation by sand@TiO_2-SiO_2@TiO_2 photocatalysts*

Electron paramagnetic resonance (EPR), fluorescence, and HPLC-MS studies were performed to understand the mechanism of PET degradation under photocatalytic conditions. Thus, electron paramagnetic resonance (EPR) experiments with sand@TiO_2-SiO_2@TiO_2 3T photocatalyst in the presence of the spin-trapping DMPO confirmed that the photocatalyst generates hydroxyl radicals ($^{\bullet}$OH) under irradiation. Hence, it was observed that the generation of DMPO-OH adduct, which displays a quartet signal (intensity 1:2:2:1) with hyperfine coupling constants of A_N = 14.9 G and A_H = 14.9 G, was light-dependent (Fig. S15). Consequently, as expected for the TiO_2 photocatalyst, the hydroxyl radical is the main reactive intermediate involved in the PET degradation. However, we cannot discard additional reactions between PET and the photogenerated holes at the photocatalyst surface.

To gain further insight into oxidation processes within the PET structure during photocatalytic treatment, the output water of the three flow rates was analyzed by high-performance liquid chromatography coupled to mass spectrometry (LC-MS) to identify photoproducts of the PET degradation. Results revealed the formation of smaller, water-soluble products, consistent with oligomeric PET fragments (Figs. S16 and S17). Among these, a collection of isomeric products with a mass/charge compatible with hydroxylated derivatives of the terephthalic moiety (*m/z* 702) was tentatively identified, providing direct evidence of $^{\bullet}$OH incorporation into the aromatic ring of PET (Fig. S17) [72]. The formation of these hydroxylated PET-derived oligomers was mainly observed at the intermediate flow rate of 0.1 L h^{-1} (τ, 80 min), whereas their signal intensity markedly decreased at 0.05 L h^{-1} (τ, 160 min), consistent with the higher mineralization achieved at longer residence times. This suggests that the species detected at m/z 702 correspond to transient oxidation intermediates generated after partial PET chain cleavage and hydroxylation. In contrast, at 1.0 L h^{-1} (τ, 8 min), the shorter irradiation/contact time likely limits sufficient PET oxidation for



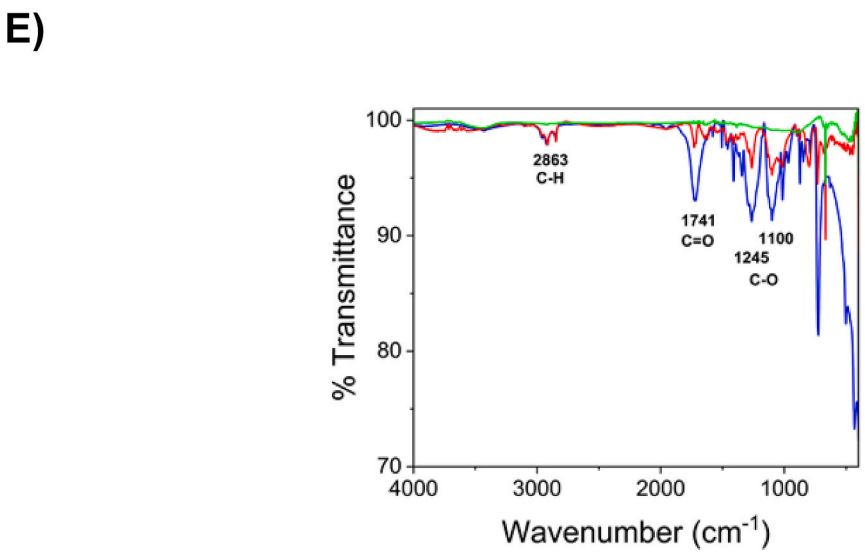


Fig. 5. (A-D) FESEM images of the filtrates corresponding to wastewater in the inlet tank of the photoreactor (water input) and to output water from the photoreactor packed with the sand@TiO_2-SiO_2@TiO_2 photocatalyst 3T after irradiation at different flow rates as indicated. (E) FTIR spectra (% transmittance) of filtrate obtained from the output water of photoreactor under dark (red), and upon irradiation (green) using photocatalyst sand@TiO_2-SiO_2@TiO_2 3T and a flow rate of 0.05 L h^{-1}.The trace corresponding to the input water sample (blue) is included for comparison.

detectable intermediate accumulation, while at 0.05 L h^{-1} these intermediates undergo further oxidative fragmentation and mineralization. These observations are consistent with a progressive ROS-mediated PET degradation pathway involving hydroxylation and oxidative cleavage of the polymer chains, generating oxidized terephthalate-containing oligomers together with smaller aliphatic fragments derived from the ethylene glycol moieties. Although these low-molecular-weight intermediates were not individually quantified, their further oxidation into short-chain oxygenated compounds and small organic acids is consistent with previously reported photocatalytic degradation pathways for aromatic acids (Fig. 6) [44,73–77].

To validate the proposed hydroxylation pathway, terephthalic acid (TPA), a structural subunit of PET, was used as a model substrate in fluorescence experiments. Irradiation of the disodium salt of TPA, in the presence of the sand@TiO_2-SiO_2@TiO_2 photocatalyst 3T under UVA, produced the characteristic fluorescence emission band of 2-

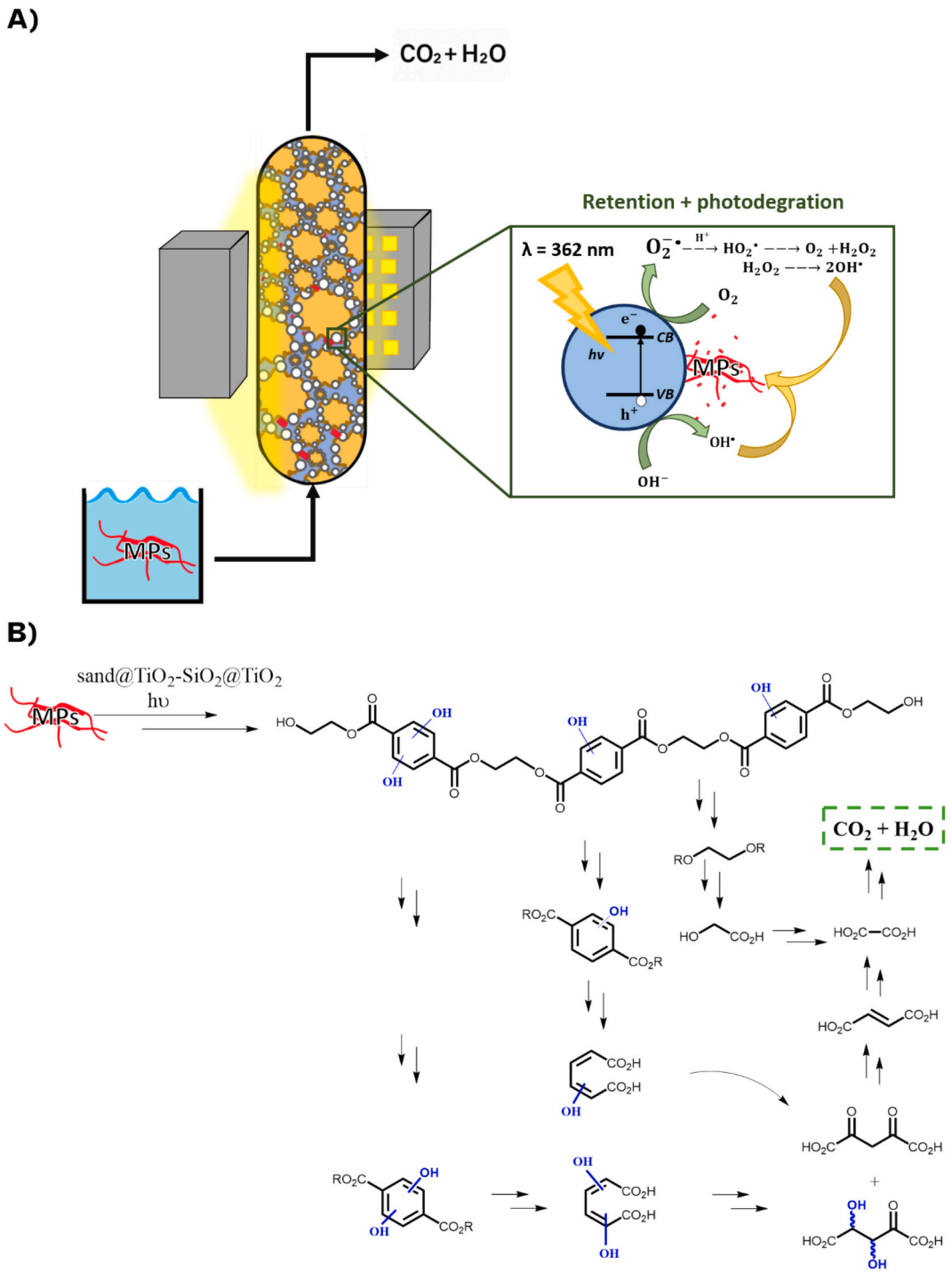


Fig. 6. A) Schematic representation of the photocatalytic MPs degradation in the presence of the sand@TiO_2-SiO_2@TiO_2 photocatalyst 3T. B) Plausible photodegradation mechanism.

hydroxyterephthalic salt at 425 nm (λ_{exc} = 315 nm), whereas no emission was detected in the corresponding dark control, confirming that hydroxyl radicals generated by the photocatalyst react with aromatic terephthalate units (Fig. S18) [78]. These findings collectively support a $^\bullet$OH-mediated oxidative cleavage pathway, accounting for the progressive depolymerization and mineralization of PET in real wastewater matrices (Fig. 6).

3.6. Comparison with other works

Currently, only a limited number of studies have addressed the photocatalytic degradation of PET micro- and nanoplastics using TiO_2-based materials. These studies employ catalysts ranging from nanoparticles and nanofibers to microfibers and particulate composites, often combined with additional oxides, metals, or different supports while maintaining TiO_2 as the active centre (Table 2). Every reported system operates in batch mode under visible or UV–visible irradiation, typically relying on heterojunctions or modified TiO_2 to extend light absorption. Xe or LED lamps delivering irradiances of up to *ca.* 600 mW cm^{-2} and irradiation times of 5–120 h are commonly used, and degradation is generally evaluated by weight loss, SEM, FTIR, UV–Vis, ^{1}H NMR, or COD measurements. Reported removal efficiencies span a wide range

Table 2
Comparative table of other works attempting microplastic photodegradation ordered chronologically.

TiO_2 appearance	PET appearance	Reactor mode	Water matrix	Additives/ adjustment	Light source	Reaction/ residence time[a]	Characterization	Efficiency	References
Bi_2O_3@N-TiO_2	Microfibers	Batch	Synthetic	pH 9	Visible (Xe lamp, 100 mW cm^{-2})	48 h	Weight loss, SEM, DSC, GC–MS	10%	Zhou et al. (2022) [64]
C,N-TiO_2 /SiO_2	Microparticles	Batch	Synthetic	pH 6–8	Visible (LED, 50 mW cm^{-2})	120 h	Weight loss, FTIR, DSC, TGA, SEM	9–16%	Ariza-Tarazona et al. (2023) [45]
TiO_2 /MIL-100 (Fe)	Nanoparticles	Batch	Synthetic	pH 3	Visible (Xe lamp, 3 mW cm^{-2})	5 h	FTIR, Turbidity, TOC, SEM	Not determined	Rojas-Guerrero et al. (2023) [50]
Ni_5P_4/TiO_2/C nanofibers	Microfibers	Batch	Synthetic	Alkaline pretreatment (5 M KOH)	UV–Visible (Hg lamp, 500 W)	12 h	Weight loss, ^1H NMR	6%	Peng et al. (2023) [65]
Ni_2P–Cu_3P/TiO_2/C nanofibers	Microfibers	Batch	Synthetic	Alkaline pretreatment (10 M KOH)	Visible (Xe lamp, 500 W)	48 h	Weight loss, ^1H NMR,	15–18%	Qu et al. (2024) [66]
$(Al_2O_3)_{0.75}TiO_2$ particles	Powder	Batch	Synthetic	0.1% NaOH	Visible (LED, 4 W)	8 h	COD, UV–Vis	41%	Camacho-González et al. (2025) [67]
CuO/TiO_2 nanocomposite	Granules and films	Batch	Synthetic	Alkaline pretreatment or laser	Visible (Xe lamp, 600 mW cm^{-2})	2 h	Weight loss, SEM, FTIR	97%	Sun et al. (2025) [68]
Sand@TiO_2-SiO_2@TiO_2 photocatalyst 3T	Microfibers and nanofibers	Continuous-flow	Real laundry wastewater	None (near-neutral pH)	UVA LED (362 nm, 260 mW cm^{-2})	160 min (0.05 $L{\cdot}h^{-1}$)	COD, TOC, weight loss, turbidimetry, FTIR, FESEM, LC-MS	100% *	This work

[a] Only in this work, "reaction residence time" corresponds to "hydraulic residence time" under continuous-flow conditions ($\tau = V/Q$).
* 100% removal with 95% of MPs mineralization.

(approximately 6–97%), but they are often derived from a limited set of analytical descriptors and, in many cases, primarily reflect polymer transformation or fragmentation rather than comprehensive mineralization. Direct comparison between reported degradation efficiencies remains difficult due to the current lack of harmonized analytical methodologies in the microplastics photocatalysis literature. Different studies employ substantially different evaluation criteria, including weight loss, morphological changes, spectroscopic modifications, COD, TOC, turbidity, or microscopy analyses, which do not necessarily correspond to equivalent degrees of degradation or mineralization. Consequently, reliable assessment of MPs' photocatalytic treatment cannot rely on a single analytical parameter alone, but instead requires the combination of complementary methodologies capable of distinguishing true mineralization from partial oxidation, fragmentation, or nanoplastic formation [79].

A further common feature of these batch protocols is the use of chemically assisted conditions to facilitate PET breakdown, such as strong alkaline pre-treatments (*e.g.*, 5–10 M KOH) [65,68], or photocatalytic reactions carried out in markedly basic [45,67,68], acidic [50] or surfactant-containing media (*e.g.*, CTAB) [66]. While such strategies can accelerate chain scission and improve apparent degradation in model systems, they increase operational complexity and chemical consumption, and do not necessarily reflect the realistic compositions of domestic wastewater. In contrast, the system reported here operates directly on real domestic laundry wastewater (without detergent) at near-neutral pH, without pH adjustment or addition of oxidants, bases, acids, or surfactants, in a matrix characterized by high hardness and ionic strength.

From a reactor and materials design perspective, most previous studies rely on TiO_2 suspensions or finely divided powders, which maximize apparent surface area but are poorly suited for continuous-flow operation and require post-treatment separation of the photocatalyst from the treated water. The sand@TiO_2-SiO_2@TiO_2 photocatalyst 3T adopts a different strategy by immobilizing the TiO_2 active phase on a millimetric sand matrix decorated with TiO_2-coated SiO_2 microspheres. This configuration combines high interfacial contact area with favorable hydraulic behavior and low pressure drop under continuous-flow operation. Pressure-drop measurements across the packed bed yielded values of 0.13 bar at 1.0 L h^{-1} and 0.10 bar for the lower flow rates (0.1 and 0.05 L h^{-1}), supporting the adequate continuous-flow operability of the reactor configuration without the need for catalyst recovery from the effluent.

Under these conditions, the present system, the first one operating in continuous flow, achieves complete removal of PET microplastics from the effluent and approximately 95% overall mineralization of the initial microplastic load in 160 min of effective hydraulic residence time at a flow rate of 0.05 L h^{-1}, using a moderate UVA LED irradiance of *ca.* 260 mW cm^{-2} (Table 1). This performance reflects a different operational regime compared to batch suspension systems, in which limited and non-uniform contact between buoyant or sedimenting plastic particles and dispersed photocatalysts can result in incomplete degradation and the accumulation of smaller plastic fragments, even after prolonged irradiation. Moreover, treatment efficiency in this work is assessed using a broad and consistent analytical portfolio (COD, TOC, gravimetry, turbidimetry, FTIR, FESEM, and LC-MS), allowing clear discrimination between true mineralization and mere morphological or molecular-level modification of the polymer. However, further reactor optimization will be necessary before scaling up the system. In its present configuration, the photoreactor consumes approximately 5.76 kWh to mineralize 1 L of water containing 31 mg of PET MPs. This value should be regarded as preliminary, as significant improvements in photon utilization remain possible. Notably, the current reactor design incorporates lamps with two LED strips, although the column diameter employed here would likely require only a single strip to achieve sufficient irradiation. Therefore, the energy consumption could potentially be reduced by close to 50% through a more efficient lighting configuration. Moreover, reactor optimization will require minimizing potential axial irradiance gradients along the 50 cm packed bed to improve volumetric photon

utilization throughout the reactor and reduce the formation of partially illuminated or dark regions under continuous-flow operation. In addition, reflective surfaces around the column can also improve overall photonic efficiency.

In continuous-flow operation, reactor throughput can be enhanced through the parallel integration of modular units equipped with columns up to 100 cm in length. This strategy would enable higher processing capacities with minimal impact on pressure drop, while preserving sufficient residence times and effective photocatalytic contact.

In parallel, optimization of bed porosity and sand particle size distribution could further enhance MPs retention and catalyst-particle interaction while maintaining acceptable permeability and avoiding excessive pressure drop.

4. Conclusions

A new sand-based composite photocatalyst (sand@TiO_2-SiO_2@TiO_2) specifically designed for continuous-flow removal and mineralization of microplastics is presented. The material architecture integrates a scalable TiO_2-coated sand support with covalently anchored TiO_2-coated SiO_2 microspheres, combining the mechanical robustness and filtration capacity of millimetric sand with an increased density of accessible photocatalytic sites, thereby enabling stable continuous-flow operation without catalyst dispersion or post-treatment recovery. It has been tested for the mineralization of PET microplastics from real domestic laundry wastewater generated without detergent addition, at near-neutral pH and high ionic strength. When implemented in a UVA LED tubular photoreactor and fed with 2 L of real wastewater, the system exhibited a strong dependence on residence time. At a flow rate of 0.05 L h^{-1}, complete removal of detectable PET microplastics from the effluent was achieved together with an overall mineralization degree of *ca.* 95% of the initial microplastic load. This performance was established through a comprehensive analytical approach (COD, TOC, gravimetry, turbidimetry, FTIR, FESEM, and a dedicated recovery protocol), demonstrating that most of the PET retained by the sand-based filter is oxidized within the packed bed rather than merely physically trapped, thereby minimizing the release of smaller secondary fragments, such as nanoplastics, into the treated effluent. Notably, these results were obtained under continuous-flow operation using an immobilized photocatalyst and real wastewater, without pH adjustment or chemical additives, in contrast to most TiO_2-based systems reported under batch conditions. Moreover, the flow configuration provides operational flexibility by controlling residence time and treated volume, offering clear opportunities for process optimization and facilitating integration into existing industrial or municipal wastewater treatment systems. Mechanistic analyses (EPR, LC-MS, and fluorescence) indicate that PET degradation proceeds mainly *via* hydroxyl radical-mediated oxidation under UVA irradiation.

CRediT authorship contribution statement

Carlos Company-Domenech: Investigation, Formal analysis. **Alberto Blazquez-Moraleja:** Writing – original draft, Supervision, Funding acquisition, Formal analysis. **Francisco Bosca:** Writing – review & editing, Validation, Supervision, Project administration, Investigation, Funding acquisition, Conceptualization. **M. Luisa Marin:** Writing – review & editing, Validation, Supervision, Project administration, Investigation, Funding acquisition, Conceptualization.

Declaration of competing interest

The authors declare that they have no known competing financial interests or personal relationships that could have influenced the work reported in this paper.

Acknowledgments

This research was supported by the Spanish Ministry of Science and Innovation through grants TED2021-131952B-I00, PDC2022-133426-I00, and CEX2021-001230-S, funded by MCIN/AEI/10.13039/501100011033. Additional financial support was provided by the Generalitat Valenciana through the CLEAN-LAGOON project (PROMETEO/CIPROM-2024-49), the Agencia Valenciana de la Innovación (AVI, grant 20220826/UCIE-ITQ), and the Ayuda a Primeros Proyectos de Investigación (PAID-06-24) from the Universitat Politècnica de València. The authors also acknowledge the Generalitat Valenciana and the European Union for co-funding the postdoctoral contract of A.B.M. (CIAPOS/2023/201) through the European Social Fund Plus (ESF+) Operational Program 2021–2027. C.C·D acknowledges the Universitat Politècnica de València for the Predoctoral FPI fellowship (FPI-UPV/Subprograma 2) and the Spanish Catalysis Society for the master's thesis scholarship.

Appendix A. Supplementary data

Chemicals, reagents, instrumentation, synthesis of photocatalysts, collection and characterization of real samples containing microplastics, photodegradation experiments, characterization of materials, characterization of MPs, and a protocol for recovering and evaluating the retained matter. Supplementary data to this article can be found online at doi:https://doi.org/10.1016/j.cej.2026.180838.

Data availability

Data will be made available on request.

References

[1] P. Pathak, S. Sharma, S. Ramakrishna, Circular transformation in plastic management lessens the carbon footprint of the plastic industry, Mater. Today Sustain. 22 (2023) 100365.
[2] J. Barrett, Z. Chase, J. Zhang, M.M.B. Holl, K. Willis, A. Williams, B.D. Hardesty, C. Wilcox, Microplastic pollution in deep-sea sediments from the Great Australian Bight, Front. Mar. Sci. 7 (2020) 576170.
[3] I. Nabi, A.U.R. Bacha, F. Ahmad, L. Zhang, Application of titanium dioxide for the photocatalytic degradation of macro- and Micro-plastics: a review, J. Environ. Chem. Eng. 9 (2021) 105964.
[4] V. Kaing, Z. Guo, T. Sok, D. Kodikara, F. Breider, C. Yoshimura, Photodegradation of biodegradable plastics in aquatic environments: current understanding and challenges, Sci. Total Environ. 911 (2024) 168539.
[5] X. Liu, H. Shi, B. Xie, D.D. Dionysiou, Y. Zhao, Microplastics as both a sink and a source of bisphenol A in the marine environment, Environ. Sci. Technol. 53 (2019) 10188–10196.
[6] C. Wang, J. Zhao, B. Xing, Environmental source, fate, and toxicity of microplastics, J. Hazard. Mater. 407 (2021) 124357.
[7] K. Duis, A. Coors, Microplastics in the aquatic and terrestrial environment: sources (with a specific focus on personal care products), fate and effects, Environ. Sci. Eur. 28 (2016) 1–25.
[8] K.I. John, M.O. Omorogie, A.A. Bayode, A.T. Adeleye, B. Helmreich, Environmental microplastics and their additives—a critical review on advanced oxidative techniques for their removal, Chem. Pap. 77 (2023) 657–676.
[9] T.J. Park, S.H. Lee, M.S. Lee, J.K. Lee, S.H. Lee, K.D. Zoh, Occurrence of microplastics in the Han River and riverine fish in South Korea, Sci. Total Environ. 708 (2020) 134535.
[10] E.C. Minor, R. Lin, A. Burrows, E.M. Cooney, S. Grosshuesch, B. Lafrancois, An analysis of microlitter and microplastics from Lake Superior Beach sand and surface-water, Sci. Total Environ. 744 (2020) 140824.
[11] H. Nakano, M.B. Alfonso, S. Jandang, K. Imai, H. Arakawa, Microplastic pollution indexes in the coastal and open ocean areas around Japan, Reg. Stud. Mar. Sci. 69 (2023) 103287.
[12] C. Blair Crawford, B. Quinn, Microplastic Pollutants, Elsevier, 2016.
[13] Y. Jin, J. Xia, Z. Pan, J. Yang, W. Wang, Z. Fu, Polystyrene microplastics induce microbiota dysbiosis and inflammation in the gut of adult zebrafish, Environ. Pollut. 235 (2018) 322–329.
[14] L. Lei, S. Wu, S. Lu, M. Liu, Y. Song, Z. Fu, H. Shi, K.M. Raley-Susman, D. He, Microplastic particles cause intestinal damage and other adverse effects in zebrafish *Danio rerio* and nematode *Caenorhabditis elegans*, Sci. Total Environ. 619–620 (2018) 1–8.
[15] Y. Lu, Y. Zhang, Y. Deng, W. Jiang, Y. Zhao, J. Geng, L. Ding, H. Ren, Uptake and accumulation of polystyrene microplastics in zebrafish (danio Rerio) and toxic effects in liver, Environ. Sci. Technol. 50 (2016) 4054–4060.

[16] M. Oliviero, T. Tato, S. Schiavo, V. Fernández, S. Manzo, R. Beiras, Leachates of micronized plastic toys provoke Embryotoxic effects upon sea urchin Paracentrotus Lividus, Environ. Pollut. 247 (2019) 706–715.
[17] A. Ragusa, A. Svelato, C. Santacroce, P. Catalano, V. Notarstefano, O. Carnevali, F. Papa, M.C.A. Rongioletti, F. Baiocco, S. Draghi, E. D'Amore, D. Rinaldo, M. Matta, E. Giorgini, Plasticenta: first evidence of microplastics in human placenta, Environ. Int. 146 (2021) 106274.
[18] P. Schwabl, S. Koppel, P. Konigshofer, T. Bucsics, M. Trauner, T. Reiberger, B. Liebmann, Detection of various microplastics in human stool: a prospective case series, Ann. Intern. Med. 171 (2019) 453–457.
[19] V. Bhatt, J.S. Chauhan, Microplastic in freshwater ecosystem: bioaccumulation, trophic transfer, and biomagnification, Environ. Sci. Pollut. Res. Int. 30 (2023) 9389–9400.
[20] D. He, K. Bristow, V. Filipović, J. Lv, H. He, Microplastics in terrestrial ecosystems: a scientometric analysis, Sustainability 12 (2020) 8739.
[21] F. Miao, Y. Liu, M. Gao, X. Yu, P. Xiao, M. Wang, S. Wang, X. Wang, Degradation of polyvinyl chloride microplastics via an electro-Fenton-like system with a TiO2/graphite cathode, J. Hazard. Mater. 399 (2020) 123023.
[22] L. Yao, H. Yang, Z. Chen, M. Qiu, B. Hu, X. Wang, Bismuth oxychloride-based materials for the removal of organic pollutants in wastewater, Chemosphere 273 (2021) 128576.
[23] S. Shabbir, M. Faheem, N. Ali, P.G. Kerr, L.F. Wang, S. Kuppusamy, Y. Li, Periphytic biofilm: an innovative approach for biodegradation of microplastics, Sci. Total Environ. 717 (2020) 137064.
[24] G. Gandon-Ros, S.S. Nuñez, N. Ortuño, I. Aracil, M.F. Gómez-Rico, J.A. Conesa, A win–win combination to inhibit persistent organic pollutant formation via the co-incineration of polyvinyl chloride e-waste and sewage sludge, Polymers (Basel). 13 (2021) 835.
[25] A.U.R. Bacha, I. Nabi, L. Zhang, Mechanisms and the engineering approaches for the degradation of microplastics, ACS EST Eng. 1 (2021) 1481–1501.
[26] P.S. Konstas, C. Kosma, I. Konstantinou, T. Albanis, Photocatalytic treatment of pharmaceuticals in real hospital wastewaters for effluent quality amelioration, Water 11 (2019) 2165.
[27] D.B. Miklos, C. Remy, M. Jekel, K.G. Linden, J.E. Drewes, U. Hübner, Evaluation of advanced oxidation processes for water and wastewater treatment – a critical review, Water Res. 139 (2018) 118–131.
[28] S. Sharma, S. Basu, N.P. Shetti, M.N. Nadagouda, T.M. Aminabhavi, Microplastics in the environment: occurrence, perils, and eradication, J. Chem. Eng. 408 (2021) 127317.
[29] S. Kim, A. Sin, H. Nam, Y. Park, H. Lee, C. Han, Advanced oxidation processes for microplastics degradation: a recent trend, J. Adv. Chem. Eng. 9 (2022) 100213.
[30] K. Zhang, A.H. Hamidian, A. Tubić, Y. Zhang, J.K.H. Fang, C. Wu, P.K.S. Lam, Understanding plastic degradation and microplastic formation in the environment: a review, Environ. Pollut. 274 (2021) 116554.
[31] A. Al Mamun, T.A.E. Prasetya, I.R. Dewi, M. Ahmad, Microplastics in human food chains: food becoming a threat to health safety, Sci. Total Environ. 858 (2023) 159834.
[32] T. Bond, V. Ferrandiz-Mas, M. Felipe-Sotelo, E. van Sebille, The occurrence and degradation of aquatic plastic litter based on polymer physicochemical properties: a review, Crit. Rev. Environ. Sci. Technol. 48 (2018) 685–722.
[33] R.J. Mueller, Biological degradation of synthetic polyesters-enzymes as potential catalysts for polyester recycling, Process Biochem. 41 (2006) 2124–2128.
[34] I.E. Napper, R.C. Thompson, Release of synthetic microplastic plastic Fibres from domestic washing machines: effects of fabric type and washing conditions, Mar. Pollut. Bull. 112 (2016) 39–45.
[35] F. De Falco, E. Di Pace, M. Cocca, M. Avella, The contribution of washing processes of synthetic clothes to microplastic pollution, Sci. Rep. 9 (2019) 6633.
[36] L. Tian, E. Skoczynska, R.J. van Putten, H.A. Leslie, G.J.M. Gruter, Quantification of polyethylene terephthalate Micro- and Nanoplastics in domestic wastewater using a simple three-step method, Sci. Total Environ. 857 (2023) 159209.
[37] M.A. Hanif, N. Ibrahim, F.A. Dahalan, U.F. Md Ali, M. Hasan, A.A. Jalil, Microplastics and Nanoplastics: recent literature studies and patents on their removal from aqueous environment, Sci. Total Environ. 810 (2022) 152115.
[38] K. Hu, P. Zhou, Y. Yang, T. Hall, G. Nie, Y. Yao, X. Duan, S. Wang, Degradation of microplastics by a thermal Fenton reaction, ACS EST Eng. 2 (2022) 110–120.
[39] J.M. Lee, R. Busquets, I.C. Choi, S.H. Lee, J.K. Kim, L.C. Campos, Photocatalytic degradation of polyamide 66: evaluating the feasibility of photocatalysis as a microfibre-targeting technology, Water 12 (2020) 3551.
[40] T. Easton, V. Koutsos, E. Chatzisymeon, Removal of polyester fibre microplastics from wastewater using a UV/H2O2 oxidation process, J. Environ. Chem. Eng. 11 (2023) 109057.
[41] J. Lin, D. Yan, J. Fu, Y. Chen, H. Ou, Ultraviolet-C and vacuum ultraviolet inducing surface degradation of microplastics, Water Res. 186 (2020) 116360.
[42] N.R. Paliwal, A.K. Mungray, Ultrasound assisted alkaline hydrolysis of poly (ethylene terephthalate) in presence of phase transfer catalyst, Polym. Degrad. Stab. 98 (2013) 2094–2101.
[43] Z. Ouyang, Y. Yang, C. Zhang, S. Zhu, L. Qin, W. Wang, D. He, Y. Zhou, H. Luo, F. Qin, Recent advances in photocatalytic degradation of plastics and plastic-derived chemicals, J. Mater. Chem. A 9 (2021) 13402–13441.
[44] Y. Wan, H. Wang, J. Liu, J. Li, W. Zhou, J. Zhang, X. Liu, X. Song, H. Wang, P. Huo, Removal of polyethylene terephthalate plastics waste via Co–CeO2 photocatalyst–activated peroxymonosulfate strategy, J. Chem. Eng. 479 (2024) 147781.
[45] M.C. Ariza-Tarazona, C. Siligardi, H.A. Carreón-López, J.E. Valdéz-Cerda, P. Pozzi, G. Kaushik, J.F. Villarreal-Chiu, E.I. Cedillo-González, Low environmental impact remediation of microplastics: visible-light photocatalytic degradation of PET microplastics using bio-inspired C,N-TiO2/SiO2 photocatalysts, Mar. Pollut. Bull. 193 (2023) 115206.
[46] M. Urso, M. Pumera, Nano/microplastics capture and degradation by autonomous nano/microrobots: a perspective, Adv. Funct. Mater. 32 (2022) 2112120.
[47] P. Chattopadhyay, M.C. Ariza-Tarazona, E.I. Cedillo-González, C. Siligardi, J. Simmchen, Combining photocatalytic collection and degradation of microplastics using self-asymmetric Pac-man TiO2, Nanoscale 15 (2023) 14774.
[48] K.K. Jaiswal, S. Dutta, I. Banerjee, C.B. Pohrmen, R.K. Singh, H.T. Das, S. Dubey, V. Kumar, Impact of aquatic microplastics and Nanoplastics pollution on ecological systems and sustainable remediation strategies of biodegradation and Photodegradation, Sci. Total Environ. 806 (2022) 151358.
[49] L. Liu, M. Xu, Y. Ye, B. Zhang, On the degradation of (micro)plastics: degradation methods, influencing factors, environmental impacts, Sci. Total Environ. 806 (2022) 151312.
[50] C.A. Rojas-Guerrero, M. Villanueva-Rodríguez, J.L. Guzmán-Mar, A. Hernández-Ramírez, E.I. Cedillo-González, F.E. Longoria Rodríguez, L. Hinojosa-Reyes, Solar photocatalytic degradation of polyethylene terephthalate Nanoplastics: evaluation of the applicability of the TiO2/MIL-100(Fe) composite material, J. Environ. Chem. Eng. 11 (2023) 110415.
[51] M.C. Ariza-Tarazona, J.F. Villarreal-Chiu, J.M. Hernández-López, J. Rivera De la Rosa, V. Barbieri, C. Siligardi, E.I. Cedillo-González, Microplastic pollution reduction by a carbon and nitrogen-doped TiO2: effect of PH and temperature in the photocatalytic degradation process, J. Hazard. Mater. 395 (2020) 122632.
[52] W. Hamd, E.A. Daher, T.S. Tofa, J. Dutta, Recent advances in photocatalytic removal of microplastics: mechanisms, kinetic degradation, and reactor design, Front. Mar. Sci. 9 (2022) 885614.
[53] O. Cabezuelo, L.N. Ponce-Gonzalez, M.L. Marin, F. Bosca, A highly efficient supported TiO2 Photocatalyst for wastewater remediation in continuous flow, Appl. Mater. Today 35 (2023) 101947.
[54] O. Cabezuelo, A. Diego-Lopez, P. Atienzar, M. Luisa Marin, F. Bosca, Optimizing the use of light in supported TiO2 photocatalysts: relevance of the shell thickness, J. Photochem. Photobiol. A 444 (2023) 114917.
[55] W. Stober, A. Fink, D. Ernst Bohn, Controlled growth of monodisperse silica spheres in the micron size range, J. Colloid Interface Sci. 26 (1968) 62–69.
[56] Y.K. Abdel-Maksoud, E. Imam, A.R. Ramadan, Sand supported TiO2 Photocatalyst in a tray photo-reactor for the removal of emerging contaminants in wastewater, Catal. Today 313 (2018) 55–62.
[57] D.A.H. Hanaor, C.C. Sorrell, Sand supported mixed-phase TiO2 Photocatalysts for water decontamination applications, Adv. Eng. Mater. 16 (2014) 248–254.
[58] C.E. Enyoh, Q. Wang, Combined experimental and molecular dynamics removal processes of contaminant phenol from simulated wastewater by polyethylene terephthalate microplastics, Environ. Technol. 45 (2024) 1183–1202.
[59] W. Xie, R. Li, Q. Xu, Enhanced photocatalytic activity of se-doped TiO2 under visible light irradiation, Sci. Rep. 8 (2018) 8752.
[60] S.K. Sharma, A.K. Misra, S. Ismail, U.N. Singh, Remote Raman Spectroscopy of Various Mixed and Composite Mineral Phases at 7.2 m Distance, . In 37th Lunar and Planetary Science Conference;, 2006.
[61] W. Wang, J. Cong, J. Deng, X. Weng, Y. Lin, Y. Huang, T. Peng, Developing effective separation of feldspar and quartz while recycling tailwater by HF pretreatment, Minerals 8 (2018) 149.
[62] B. Ingham, M.F. Toney, X-Ray Diffraction for Characterizing Metallic Films, in: Metallic Films for Electronic, Optical and Magnetic Applications, Elsevier, 2014, pp. 3–38.
[63] D. Zhou, H. Luo, F. Zhang, J. Wu, J. Yang, H. Wang, Efficient photocatalytic degradation of the persistent PET Fiber-based microplastics over Pt nanoparticles decorated N-doped TiO2 Nanoflowers, Adv. Fiber Mater. 4 (2022) 1094–1107.
[64] D. Zhou, L. Wang, F. Zhang, J. Wu, H. Wang, J. Yang, Feasible degradation of polyethylene terephthalate fiber-based microplastics in alkaline media with Bi_2O_3@N-TiO_2 Z-scheme photocatalytic system, Adv. Sustain. Syst. 6 (2022) 2100516.
[65] G. Peng, X. Qi, W. Qu, X. Shao, L. Song, P. Du, J. Xiong, Photocatalytic degradation of PET microfibers and hydrogen evolution by Ni5P4/TiO2/C NFs, Cat. Sci. Technol. 13 (2023) 5868–5879.
[66] W. Qu, G. Peng, L. Song, W. Guo, Y. Chen, P. Du, J. Xiong, Efficient and stable photocatalytic degradation of PET waste textiles through Ni2P-Cu3P/TiO2/C NFs facilitated by the synergistic effect of CTAB and p-n heterojunctions, J. Mater. Chem. C 12 (2024) 8837–8845.
[67] M.A. Camacho-González, A. Hernández-Reyes, A. Garrido-Hernández, O. Olivares-Xometl, N.V. Likhanova, I.V. Lijanova, TPA and PET photo-degradation by heterogeneous catalysis using a $(Al_2O_3)_{0.75}TiO_2$ coating, Surfaces 8 (2025) 34.
[68] A. Sun, Y. Zhao, J. Li, H. Lai, H. Li, Z. Yang, J. He, P. Pan, R. Zhang, Enhanced visible-light photocatalytic degradation of PET using CuO/TiO2 Heterostructure nanocomposites: a comprehensive study, Vacuum 240 (2025) 114602.
[69] GENERAL DE ANÁLISIS, M. Y. S. S. L. (GAMASER), *Informe de Ensayo No. 2023/055222. Analysis of Drinking Water*, Valencia (Spain), 2023.
[70] M. Funck, M.M.S. Al-Azzawi, A. Yildirim, O. Knoop, T.C. Schmidt, J.E. Drewes, J. Tuerk, Release of microplastic particles to the aquatic environment via wastewater treatment plants: the impact of sand filters as tertiary treatment, J. Chem. Eng. 426 (2021) 130933.
[71] Y.K. Song, S.H. Hong, S. Eo, W.J. Shim, The fragmentation of Nano- and Microplastic particles from thermoplastics accelerated by simulated-sunlight-mediated Photooxidation, Environ. Pollut. 311 (2022) 119847.
[72] T. Sang, C.J. Wallis, G. Hill, G.J.P. Britovsek, Polyethylene terephthalate degradation under natural and accelerated weathering conditions, Eur. Polym. J. 136 (2020) 109873.

[73] Y. Wan, H. Wang, J. Liu, X. Liu, X. Song, W. Zhou, J. Zhang, P. Huo, Enhanced degradation of polyethylene terephthalate plastics by CdS/CeO2 heterojunction Photocatalyst activated Peroxymonosulfate, J. Hazard. Mater. 452 (2023) 131375.
[74] T.D. Bui, A. Kimura, S. Ikeda, M. Matsumura, Determination of oxygen sources for oxidation of benzene on TiO_2 Photocatalysts in aqueous solutions containing molecular oxygen, J. Am. Chem. Soc. 132 (2010) 8453–8458.
[75] X. Pang, W. Chang, C. Chen, H. Ji, W. Ma, J. Zhao, Determining the TiO_2 -photocatalytic aryl-ring-opening mechanism in aqueous solution using Oxygen-18 labeled O_2 and H_2O, J. Am. Chem. Soc. 136 (2014) 8714–8721.
[76] X. Li, J.W. Cubbage, W.S. Jenks, Photocatalytic degradation of 4-Chlorophenol. 2. The 4-Chlorocatechol pathway, J. Org. Chem. 64 (1999) 8525–8536.
[77] J. Yang, J. Dai, C. Chen, J. Zhao, Effects of hydroxyl radicals and oxygen species on the 4-Chlorophenol degradation by Photoelectrocatalytic reactions with TiO2-film electrodes, J. Photochem. Photobiol. A Chem. 208 (2009) 66–77.
[78] K. Ishibashi, A. Fujishima, T. Watanabe, K. Hashimoto, Detection of active oxidative species in TiO2 Photocatalysis using the fluorescence technique, Electrochem. Commun. 2 (2000) 207–210.
[79] C. Álvarez-Fernández, M. Liras, V.A. de la Peña O'Shea, K. Mirehbar, J. Lado, J. Palma, J. Marugán, Removal of polyethylene micro(nano)plastics from water: exploring the combination of anodic oxidation and membrane microfiltration, Process. Saf. Environ. Prot. 210 (2026) 108674.